Chemistry–A European Journal

Supporting Information

# Lanthanide Identity Governs Guest-Induced Dimerization in $Ln^{III}[15\text{-}MC_{Cu^{II}N(L\text{-}pheHA)}\text{-}5])^{3+}$ Metallacrowns

Carmelo Sgarlata,* Bernadette L. Schneider, Valeria Zito, Rossella Migliore, Matteo Tegoni,* Vincent L. Pecoraro,* and Giuseppe Arena*

**Supporting Information Contents:**

## Note on Materials

Due to the long period of slow evaporation for crystallization of the metallacrown complexes, the counterions are more likely $CO_3^{2-}$ as has recently been published by Addison, et al.[1] and are less likely to be $NO_3^-$ counterions, as our group previously published.[2] Since $CO_3^{2-}$ would likely bind stronger to the MC than $NO_3^-$, we have considered the presence of carbonate in the solution on our studies and we do not believe the interpretation is impacted as to whether $NO_3^-$ or $CO_3^{2-}$ is assumed as the initial counterion in the crystals.

## ITC Experiments

Different species and combinations thereof (such as, for example, **Ln-MC**-Muc alone, **Ln-MC**-Muc with (**Ln-MC**)$_2$-Muc, **Ln-MC**-Muc with (**Ln-MC**)$_2$-Muc and **Ln-MC**(Muc)$_2$, (**Ln-MC**)$_2$ alone, **Ln-MC**-Muc with (**Ln-MC**)$_2$-Muc and (**Ln-MC**)$_2$-Muc$_2$ etc.) were tested but the data analysis consistently converged to the species and values shown in Table S1 and Figure 1 and rejected all the other models.

Typical full scan and expanded ITC titrations of Muc into **Eu-MC**, **Sm-MC** and **Nd-MC** are shown in Figure S1, S2 and S3 respectively, while a typical blank experiment is shown in Figure S4.

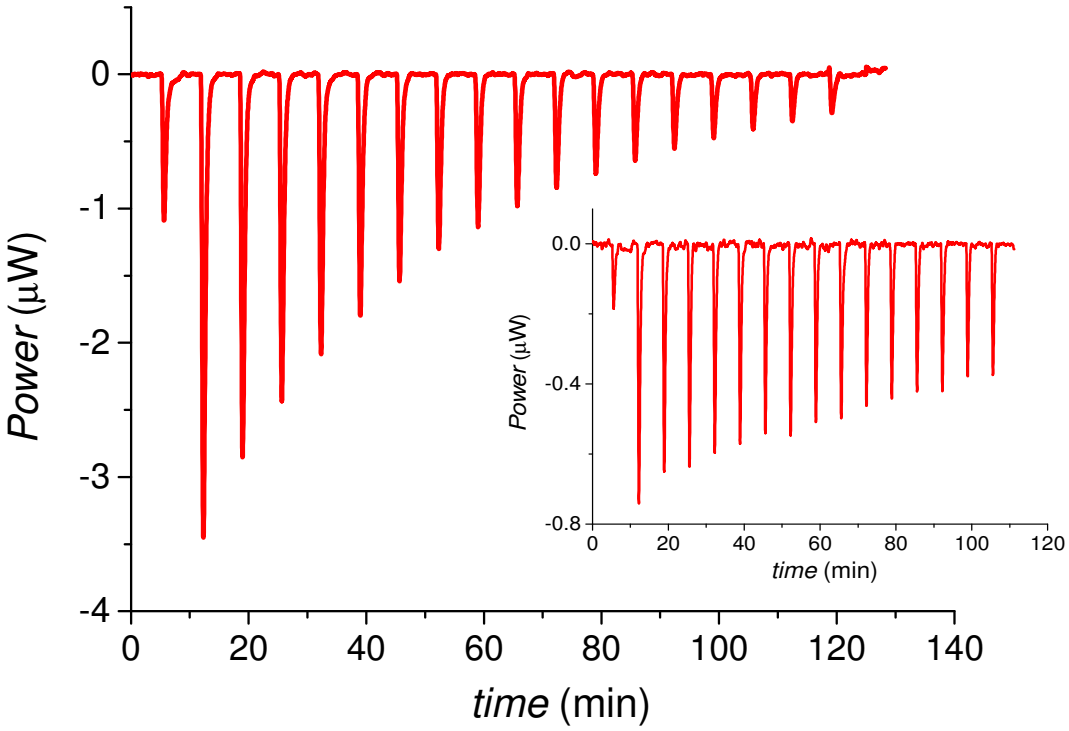


**Figure S1.** ITC titration of Muc into **Eu-MC** at 25 °C in buffered aqueous solution (pH 7.2, MOPS 50 mM). Full scan: $C_{\textbf{Eu-MC}}$ = 0.6 mM, final Muc/**Eu-MC** ratio = 5.5. Inset: expanded titration, $C_{\textbf{Eu-MC}}$ = 0.9 mM, final Muc/**Eu-MC** ratio = 0.3.

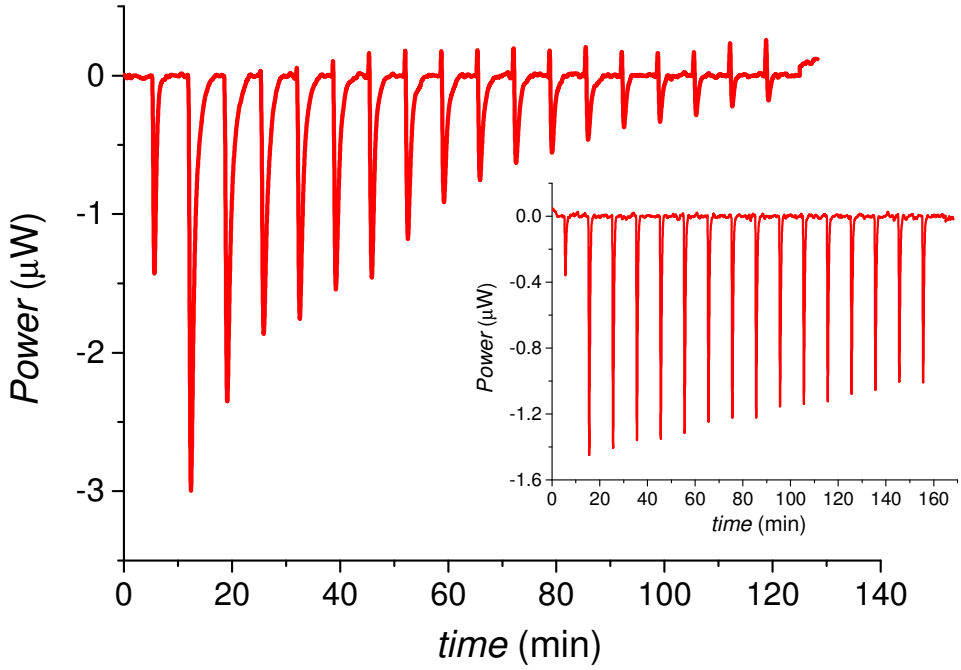


**Figure S2.** ITC titration of Muc into **Sm-MC** at 25 °C in buffered aqueous solution (pH 7.2, MOPS 50 mM). Full scan: $C_{\textbf{Sm-MC}}$ = 0.6 mM, final Muc/**Sm-MC** ratio = 5.5. Inset: expanded titration, $C_{\textbf{Sm-MC}}$ = 1 mM, final Muc/**Sm-MC** ratio = 0.3.

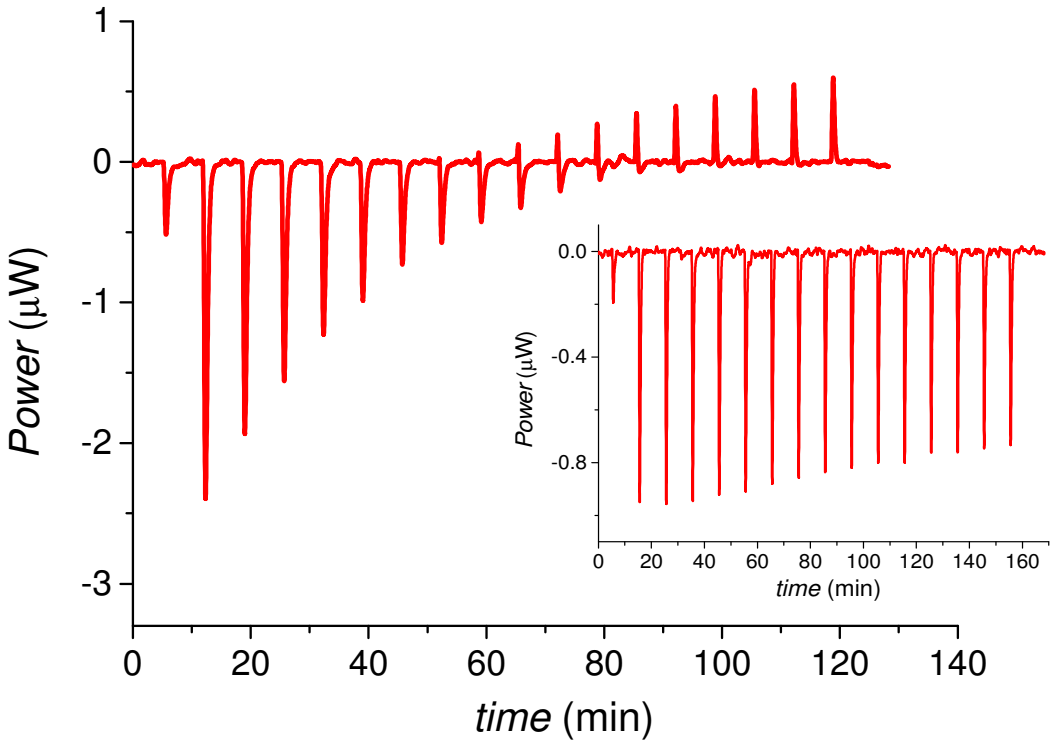


**Figure S3.** ITC titration of Muc into **Nd-MC** at 25 °C in buffered aqueous solution (pH 7.2, MOPS 50 mM). Full scan: $C_{\textbf{Nd-MC}}$ = 0.45 mM, final Muc/**Nd-MC** ratio = 6. Inset: expanded titration, $C_{\textbf{Nd-MC}}$ = 1 mM, final Muc/**Nd-MC** ratio = 0.3.

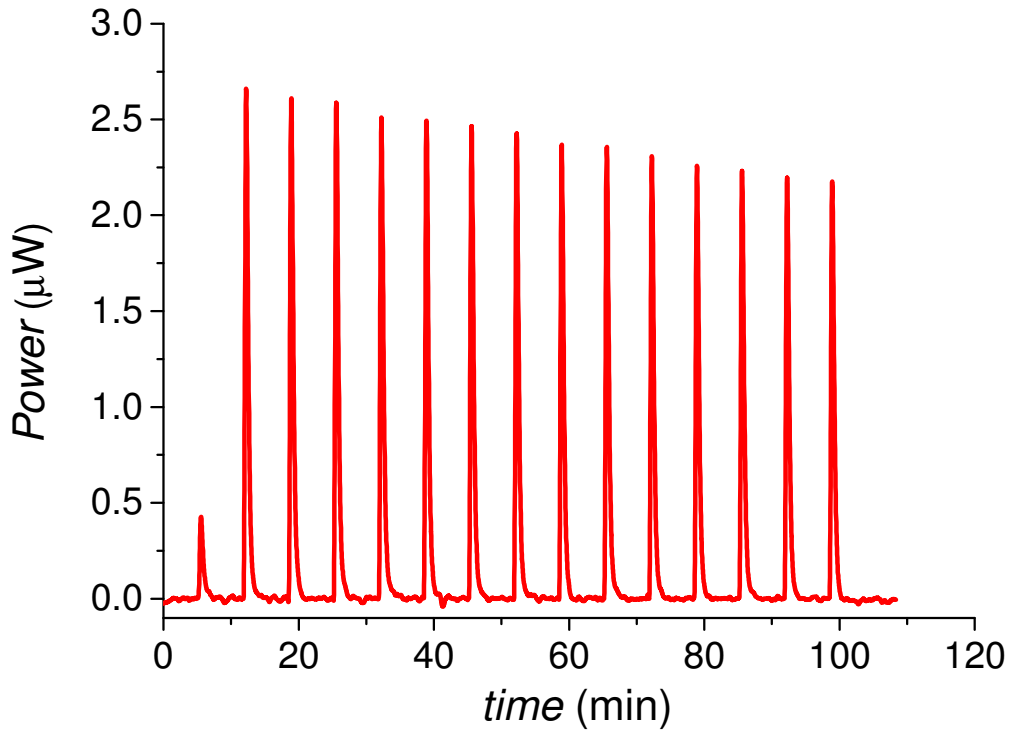


**Figure S4.** Dilution (blank) experiment: titration of Muc into a buffered aqueous solution (pH 7.2, MOPS 50 mM) at 25 ℃.

**Table S1.** Thermodynamic parameters[a] for the **Ln-MC**/Muc systems at 25 °C in buffered aqueous solution (pH 7.2, MOPS 50 mM)

| **Ln-MC** | **Reaction** | **log*K*** | **Δ*G*°** (kJ/mol) | **Δ*H*°** (kJ/mol) | ***T*Δ*S*°** (kJ/mol) |
|---|---|---|---|---|---|
| $La^{3+}$ | **MC** + Muc ⇄ (**MC**)Muc | 2.53 (4) | -14.4 | 3.89 (2) | 18.3 (7) |
| $Nd^{3+}$ | **MC** + Muc ⇄ (**MC**)Muc | 2.71 (2) | -15.5 | 6.02 (1) | 21.5 (4) |
| $Sm^{3+}$ | **MC** + Muc ⇄ (**MC**)Muc | 2.91 (3) | -16.6 | 5.90 (1) | 22.5 (6) |
| $Eu^{3+}$ | **MC** + Muc ⇄ (**MC**)Muc | 2.52 (8) | -14.4 | 10.7 (4) | 25 (2) |
| | **MC** + (**MC**)Muc ⇄ (**MC**)$_2$Muc | 3.3 (3) | -18.8 | -10 (1) | 9 (3) |
| $Gd^{3+}$ [b] | **MC** + Muc ⇄ (**MC**)Muc | 2.4 (1) | -13.7 | 16.4 (1) | 30.1 (1) |
| | **MC** + (**MC**)Muc ⇄ (**MC**)$_2$Muc | 3.4 (2) | -19.4 | -13.91 (7) | 5.5 (2) |
| $Dy^{3+}$ | **MC** + Muc ⇄ (**MC**)Muc | 2.62 (5) | -15.0 | 11.70 (2) | 26.7 (8) |
| | **MC** + (**MC**)Muc ⇄ (**MC**)$_2$Muc | 3.1 (2) | -17.7 | -5.8 (2) | 12 (2) |
| $Ho^{3+}$ | **MC** + Muc ⇄ (**MC**)Muc | 2.79 (5) | -15.9 | 7.77 (2) | 24 (1) |

[a] σ in parentheses

[b] Ref. [3]

## Pulsed-Gradient Diffusion Ordered NMR

As compared to the NMR spectra of Sm-MC and Nd-MC, the observed signal for the Eu-MC was less intense. This decreased sensitivity required more concentrated samples for the pulsed gradient spin echo experiment (6 mM was used for Eu-MC, as opposed to 2 mM, which was used for Sm-MC and Nd-MC) as well as adjustment of experimental parameters, in which a very short relaxation delay parameter was employed. While the latter parameter remained at least 5x the measured $T_1$ of the Eu-MC signal, its change to shorter values inadvertently shifted the zero-point (guest-free) Eu-MC to higher observed diffusion parameter, $D'_{obs}$ ($D'_{obs} = D_{MC}/D_{DMSO}$), an effect that has been previously documented.[4]

Peak assignments in Table S2 and Figure S5 were made consistent with the literature.[5] In general we observed the **α** peaks typically had the fastest $T_1$ relaxation times followed by **β** peaks, and slower relaxation times for the aromatic peaks (Table S2).

## $^1$H NMR and Inversion Recovery

**Table S2.** $T_1$ Inversion Recovery (s). 2 mM Ln-MC (excepting Gd-MC, which was 6 mM) in 100 mM MOPS buffer in $D_2O$ (pD 7.2 ± 0.1, pD corrected from pH reading for $D_2O$[6]). Peak assignments were made consistent with the literature following the principle that protons present closer to the paramagnetic metal centers experience the largest paramagnetic shift[5] (labeled **α** ($CHNH_2$); **β** ($CH_2$, magnetically inequivalent); and **P** for the aromatic protons of the phenyl group).

| | | α | β | β' | P | P | P |
|---|---|---|---|---|---|---|---|
| **Y** | $T_1$ (s) | 0.001 | 0.003, | 0.002 | 0.004 | 0.011 | |
| | *δ (ppm)* | *43.* | *11.5,* | *10.4* | *7.6* | *8.0* | |
| **La** | $T_1$ (s) | 0.002 | 0.004, | 0.004 | 0.006 | 0.020 | 0.025 [a] |
| | *δ (ppm)* | *41.93* | *10.2,* | *10.0* | *7.50* | *8.10* | *8.03* |
| **Nd** | $T_1$ (s) | 0.012 | 0.028, | 0.024 | 0.034 | 0.105 | |
| | *δ (ppm)* | *43.65* | *10.63,* | *10.33* | *7.47* | *8.03* | |
| **Sm** | $T_1$ (s) | 0.009 | 0.021, | 0.017 | 0.026 | 0.082 | 0.099 [a] |
| | *δ (ppm)* | *44.48* | *10.98,* | *10.53* | *7.44* | *7.99* | *7.95* |
| **Eu** | $T_1$ (s) | 0.003 | 0.007, | 0.006 | 0.009 | 0.027 | 0.031 [a] |
| | *δ (ppm)* | *44.7* | *10.9,* | *10.5* | *7.57* | *8.17* | *8.09* |
| **Gd [b] (6 mM)** | $T_1$ (s) | <0.001 | <0.001 | | | <0.001 | |
| | *δ (ppm)* | *46.* | *11.* | | | *8.2* | |
| **Tb [b]** | $T_1$ (s) | 0.003 | 0.007 | | 0.005 [c] | 0.008 | 0.011 [a] |
| | *δ (ppm)* | *45.* | *10.* | | *5.1* | *7.5* | *6.9* |
| **Dy [b]** | $T_1$ (s) | 0.003 | nd | | 0.005 [a] | 0.008 | |
| | *δ (ppm)* | *41.3* | | | *7.9* | *8.6* | |
| **Ho [b]** | $T_1$ (s) | 0.003 | 0.007, | 0.006 | 0.005 [c] | 0.009 | |
| | *δ (ppm)* | *43.* | *10.* | *~9.2* | *5.7* | *7.8* | |
| **Er** | $T_1$ (s) | 0.004 | 0.009, | 0.007 | 0.007 | 0.011 | 0.015 |
| | *δ (ppm)* | *42.9* | *11.08,* | *9.83* | *7.91* | *8.64* | *8.26* |

[a] Shoulder peak to the right of a larger aromatic peak. [b] For the most paramagnetic species (Gd, Tb, Dy, Ho) only very broad peaks are distinguishable. The values given are estimates. [c] Peak overlaps the $D_2O$ signal.

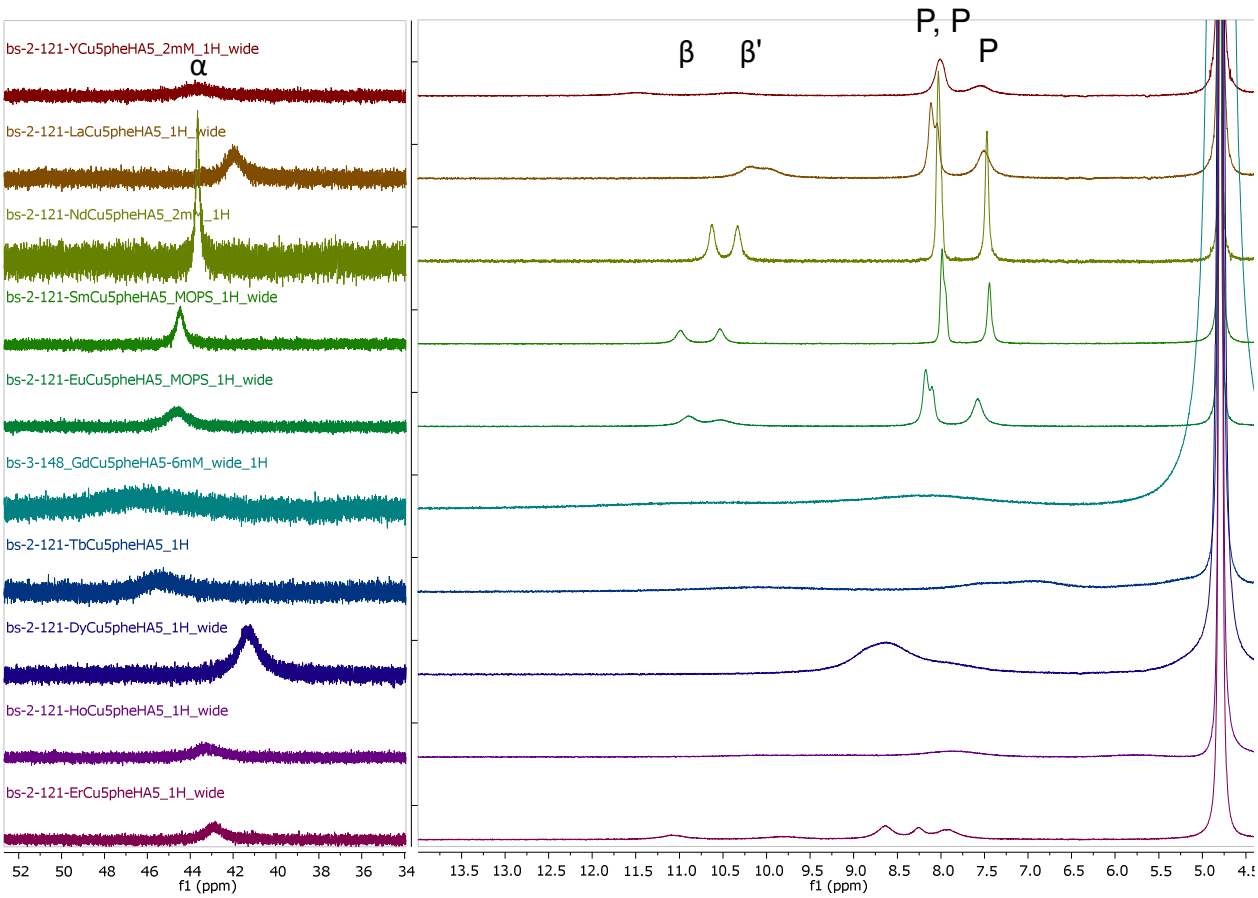


**Figure S5.** $^{1}$H NMRs of Y, La, Nd, Sm, Eu, Gd, Tb, Dy, Ho, and Er analogs of $Ln^{III}$(15-MC-$_{CuII(N)pheHA}$-5)$^{3+}$.

## Speciation Diagrams

All distribution diagram were obtained with Hyperquad Simulation and Speciation Software (HySS).[7]

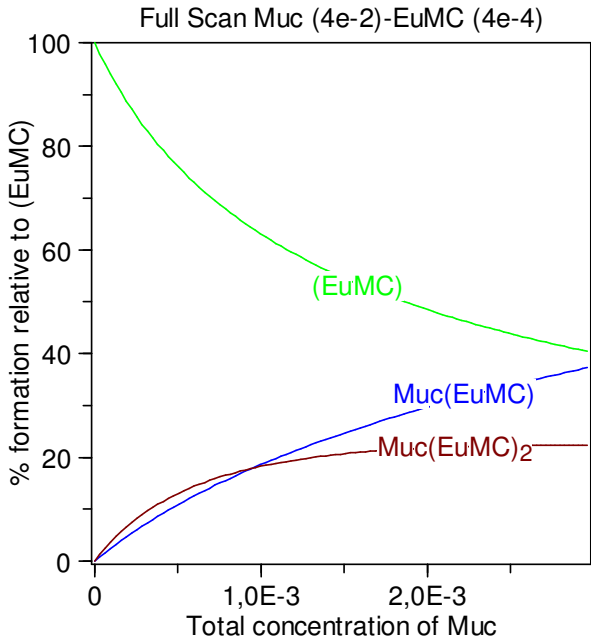


**Figure S6.** 0.4 mM EuMC titrated with 40 mM muconate: Example speciation obtained under the conditions employed for ITC. This diagram shows that the 2:1 species prevails in the initial region of ITC titrations (i.e., in the presence of excess MC) whilst the 1:1 species prevails in the remaining part of the titration. This also illustrates the need to expand the initial portion of the curve.

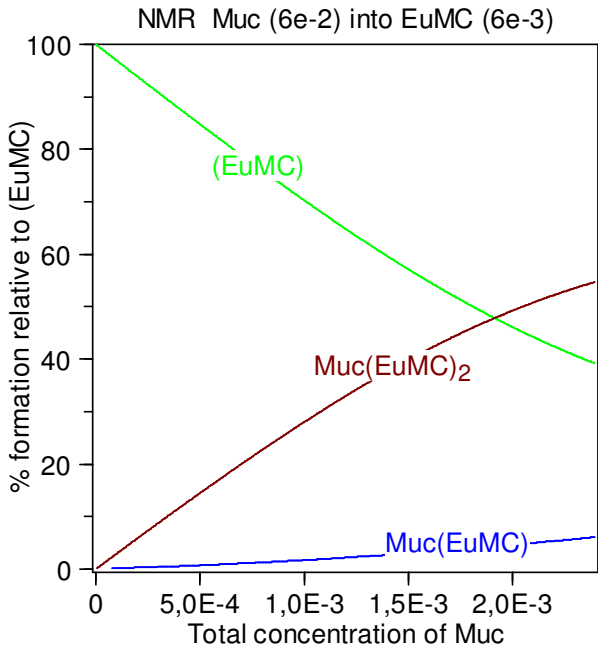


**Figure S7.** 6 mM EuMC titrated with 60 mM muconate: Speciation diagram for EuMC at the concentration used for NMR, which minimizes the formation of the 1:1 species.

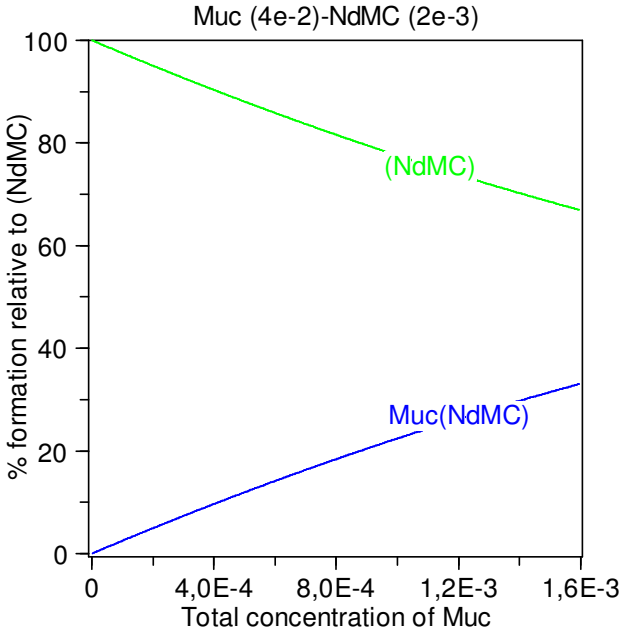


**Figure S8.** 2 mM NdMC titrated with 40 mM muconate: Speciation diagram for NdMC at the concentration used for NMR.

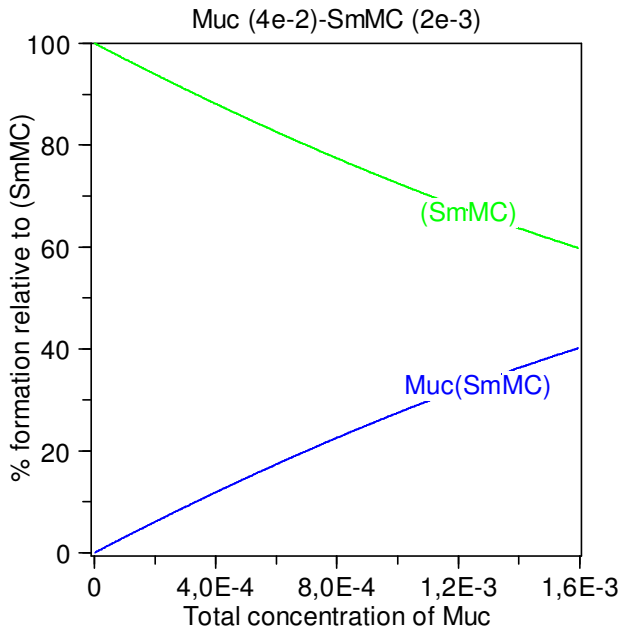


**Figure S9.** 2 mM SmMC titrated with 40 mM muconate: Speciation diagram for SmMC at the concentration used for NMR.

## $^1$H NMR Titration

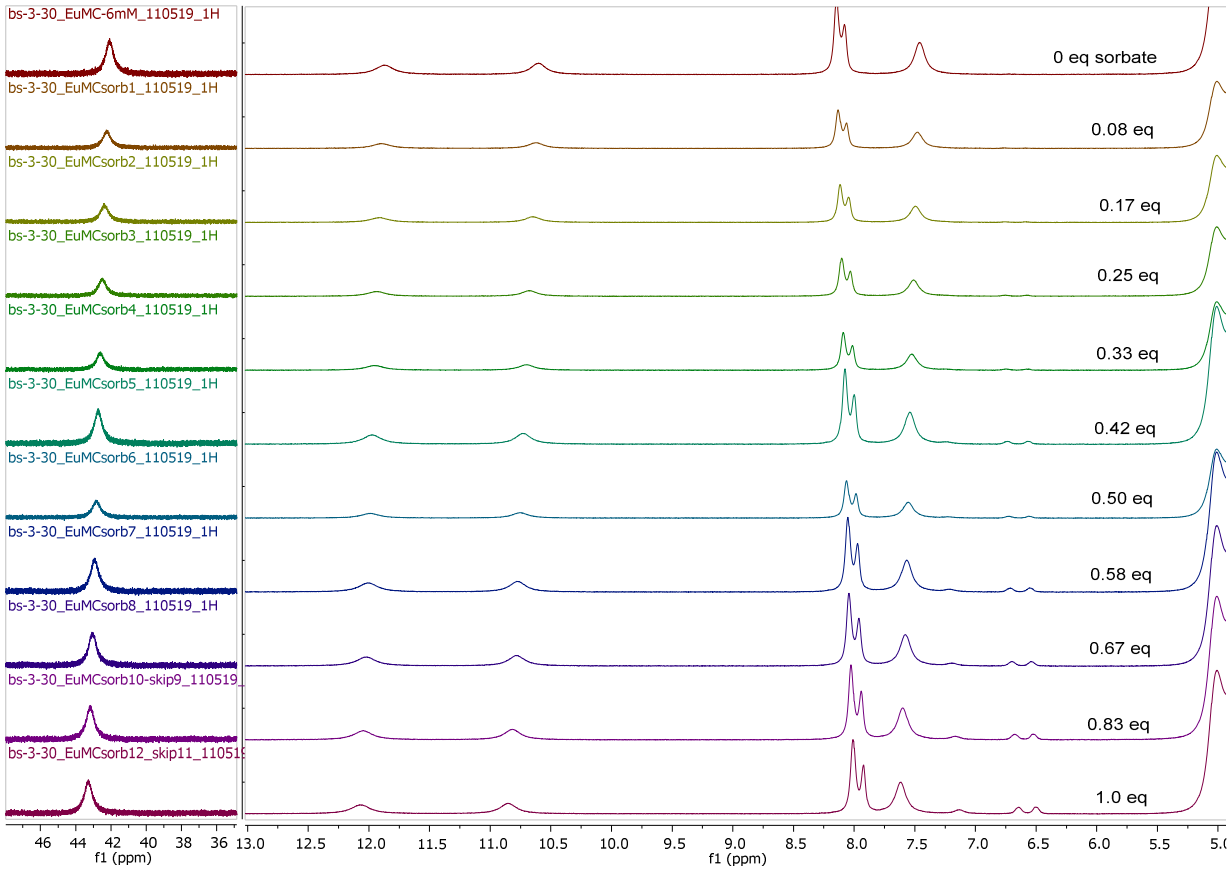


**Figure S10.** Titration of **Eu-MC** (6 mM) with potassium sorbate (60 mM) induces slight shifts $^1$H signals, which is indicative of carboxylate interaction.

## Diffusion Data Analysis

The translational diffusion constant $D_t$ is inversely proportional to hydrodynamic radius ($r_H$) as described by the Stokes Einstein equation

$$D_t = \frac{kT}{c\pi\eta r_H} \qquad (1)$$

with dependence on temperature $T$ and solution viscosity $\eta$. In eq. 1 $k$ is the Boltzmann constant, and $c$ is a numeric factor between 4 and 6, specific of that analyte.

In a PGSE experiment where the spin-echo $\tau$ parameter is kept constant and the gradient strength $G$ is varied, the intensity of an NMR signal as a function of $G$ can be expressed as

$$I_G = I_0 e^{-\rho G^2 D} = I_0 e^{-\theta G^2} \qquad (2)$$

Where $I_0$ is the intensity of the signal collected at the end of the pulse sequence at zero gradient strength ($G$ = 0). In equation 2, $\rho$ is a function of parameters or constants such as the gyromagnetic ratio of the observed nuclide, the duration of the spin echo pulses and the time interval between them. If two or more solutes are present in solution, the $\rho$ parameter is consequently the same for all molecules. The $\theta$ exponential factor ($\theta$ = - $\rho D$) is the signal decay parameter of each single resonance which can be calculated directly from PGSE data. Therefore, the ratio between the exponential decay parameters $\theta$ of the NMR signal intensity for two different solutes in the same sample reduces to the ratio between their diffusion coefficients $D$. If the two solutes are an analyte and a standard solute with unknown and known diffusion coefficients $D_{an}$ and $D_{std}$, respectively, the following equation applies, which allows a straightforward determination of $D_{an}$:

$$\frac{\theta_{an}}{\theta_{std}} = \frac{D_{an}}{D_{std}} \qquad (3)$$

In this work, NMR titrations were performed in triplicate and carried out in 1:1 MeOD:$D_2O$ buffer (100 mM MOPS, pD 7.2 ± 0.15, pD corrected from pH reading for $D_2O$,[6] prior to dilution with MeOD) with DMSO used as an internal standard. Methanol was used to avoid precipitation at the mM level concentrations that were necessary for NMR. An exception is for 6 mM **Eu-MC** – sorbate titration: only two PGSE experiments were performed for the points at 0.58 eq and 1 eq, while only 10 $G^2$ values were used for one of the experiments at 0.83 eq. NMR Spectra processing and analysis, including fit of $T_1$, was performed using MestReNova 11.0.2 software. All other least square regression analyses were performed using SPSS Statistics 26.0 software.

Experimental exponential decay parameters $\theta$ of the MC species and the standard DMSO molecule were determined by nonlinear regression analysis using SPSS Statistics software (version 26.0) by fitting PGSE $^1$H NMR data sets simultaneously using equation 4,

$$I_{calc} = c_1 I_1 e^{-\theta G^2} + c_2 I_2 e^{-\theta G^2} + c_3 I_3 e^{-\theta G^2} \qquad (4)$$

where each term of the sum corresponds to data from one of the titration experiments. The $c_1$, $c_2$ and $c_3$ coefficients are set as either 1 or 0: $c_1$ is 1 when the data come from the first titration or it is 0 when the data is from the second titration or the third, with similar treatment for $c_2$ and $c_3$ so that the equation only draws from one titration at a time. The $I_1$, $I_2$, and $I_3$ values have the same meaning of $I_0$ in eq. 2, considered for each individual titration. Using eq. 4, a single exponential decay parameter $\theta$ can be fit by SPSS by nonlinear regression analysis. This provides one single D parameter (and one single standard deviation) for a combination of titrations.

To describe diffusion of the MC-muconate system in equilibrium, the observed value of $D$ ($D_{obs}$) depends on the coefficients $D_{MC}$, $D_{1:1}$ and $D_{2:1}$, where MC, 1:1 and 2:1 refer to free MC, 1:1 MC:muconate adduct, and 2:1 the dimeric capsule, respectively. The observed $D$ ($D_{obs}$) depends also on the relative amount of each species in solution, in turn depending on the formation constants of the different species, in condition of fast chemical exchange:

$$D_{obs} = D_{MC}\chi_{MC} + D_{1:1}\chi_{1:1} + D_{2:1}\chi_{2:1} \qquad (5)$$

where $\chi$ are the molar fractions of the different species in solution. For each point of the NMR titrations, these $\chi$ values can be calculated from the formation constants provided by the calorimetric speciation model.

In the presence of small amounts of DMSO used as the standard, however, it is convenient to use the following:

$$\frac{D_{obs}}{D_{DMSO}} = \frac{D_{MC}}{D_{DMSO}}\chi_{MC} + \frac{D_{1:1}}{D_{DMSO}}\chi_{1:1} + \frac{D_{2:1}}{D_{DMSO}}\chi_{2:1} \qquad (6)$$

The reason is that the $\frac{D_{obs}}{D_{DMSO}}$ can be conveniently calculated directly as $\frac{\theta_{obs}}{\theta_{DMSO}}$, as describe by eq. 3. Hereafter we will use $D'_{obs} = \frac{D_{obs}}{D_{DMSO}} = \frac{\theta_{obs}}{\theta_{DMSO}}$, for simplicity. By rearranging eq. 6 we obtain

$$D'_{obs} = (D'_{MC} \cdot \%_{MC} + D'_{1:1} \cdot \%_{1:1} + D'_{2:1} \cdot \%_{2:1}) \cdot \frac{1}{100} \qquad (7)$$

Where % = $\chi \cdot 100$. For the Sm and Nd systems, the $D_{2:1} \cdot \%_{2:1}$ term becomes 0 since speciation demonstrated no presence of the 2:1 species. The $D'_{obs}$ values observed by NMR as a function of the muconate added could be fitted through equation 7, using the % values obtained by the calorimetric speciation. In eq. 7, $D'_{MC}$ is also a constant value which corresponds to $D'_{obs}$ of the first point of the titration.

The $D'_{obs}$ values from the three titrations of **Nd-MC** with Muconate (0-0.5 eq.; 4 points, Figure S11) were treated by least square regression analysis and $D'_{1:1}$ was determined as 0.2146(5). This value compares quite well with $D'_{MC}$ of the free NdMC which resulted, averaged over the three titrations, 0.2269(8). The slightly smaller $D'_{1:1}$ value compared to $D'_{MC}$ indicates that the former 1:1 species is just a little larger compared to the free MC, a situation compatible with the binding of a muconate anion without dimerization.

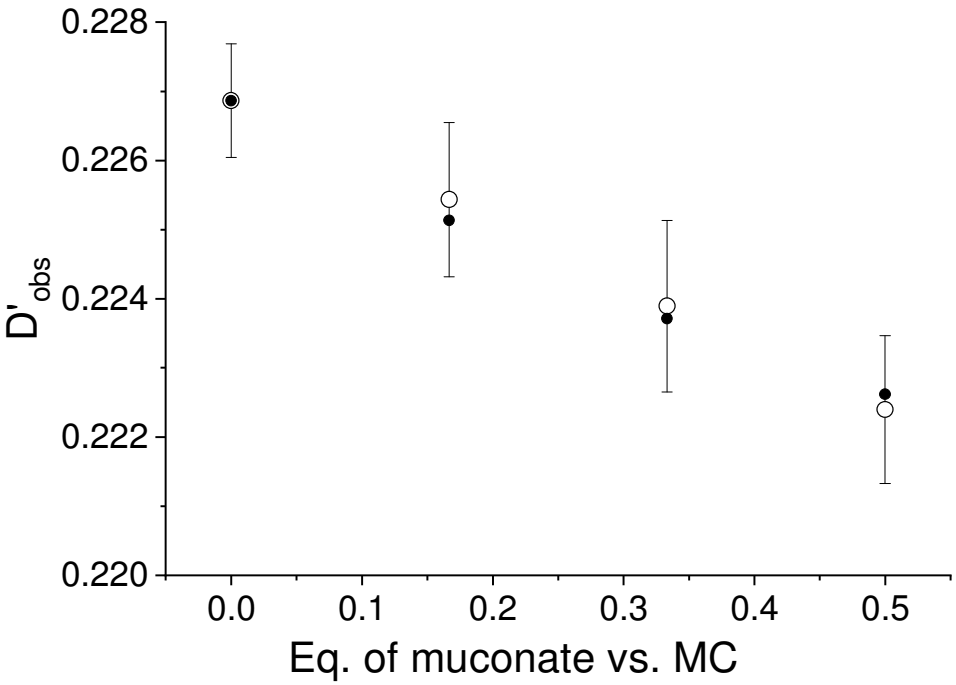


**Figure S11:** Open circles: observed $D'_{obs}$ values for the titration of **Nd-MC** with up to 0.5 eq. of muconate. Black dots: calculated D' at the points of the titration using the speciation of NdMC provided by calorimetric data (2:1 species not present in the speciation).

In Figure S12 the results of the same data treatment for the titration of **Sm-MC** with muconate is shown. $D'_{1:1}$ resulted 0.2135(9) (vs. 0.2270(10) for free SmMC). The same conclusions drawn for the Nd system can apply here.

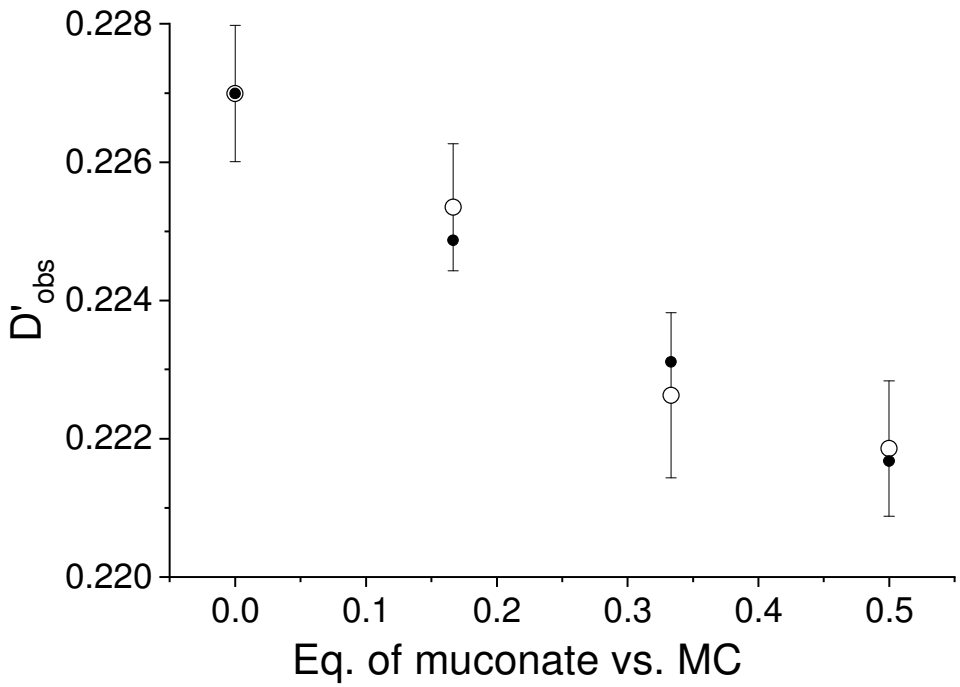


**Figure S12:** Open circles: observed $D'_{obs}$ values for the titration of **Sm-MC** with up to 0.5 eq. of muconate. Black dots: calculated D' at the points of the titration using the speciation of SmMC provided by calorimetric data (2:1 species not present in the speciation).

For the EuMC system, although we know the % of the species from the speciation of the system, $D_{1:1}$ and $D_{2:1}$ are both unknown (unlike the Sm and Nd systems in which $D_{2:1}$ is irrelevant). These values cannot be determined from independent experiments or under saturation conditions. In fact, although there exist conditions in which either the 1:1 or 2:1 species dominates over the other in terms of amount, no condition obtains 100% of one of these species in solution.

However, it is likely a good approximation to consider the diffusion features of the 1:1 species with Nd and Sm pretty similar to that of Eu, since the evaluation of their crystal structure suggest very similar dimensions.[2] The $D'_{1:1}$ value for EuMC was approximated therefore as the average of the two $D'_{1:1}$ values for Sm and Nd above, i.e., $D'_{1:1}$(Nd-Sm) = 0.2141(9). Diffusion data of Eu were treated through eq. 7, and $D'_{2:1}$ resulted 0.2091(10). This value is significantly smaller than both $D'_{MC}$ (0.2377(13)) and $D'_{1:1}$(Nd-Sm) (0.2141(9)), suggesting therefore the occurrence of an equilibrium involving MC and leading to a species of large dimensions. The results are reported in Figure 3 of the main text (black dots).

A second data treatment was carried out on diffusion NMR data for Eu, with the aim to demonstrate that the exclusion of the 2:1 from the speciation model leads to unreliable fitting of the observed data. To carry out this data treatment, the speciation of SmMC/Muconate was considered for simplicity for the calculation of calculated D. This "only 1:1" model (crossed circles in Figure 3) does not match the observed data, which must be fit by the introduction of a larger species, i.e., the 2:1 species.

The consistency of this model with theoretical expectations was then analyzed according to a Stokes-Einstein model that assumes spherical particles, with volume, *V*, proportional to the cube of the van der Waals radius, *r*, according to $V = \frac{4}{3}\pi r^3$. For a complex that dimerizes, the van der Waals volume is presumed to double, so that $V_{dimer} = 2(V_{monomer}) \propto {r_{dimer}}^3$. This corresponds to an increase of the mean van der Waals radius by a factor equal to $\sqrt[3]{2}$= 1.26, with a corresponding decrease in diffusion coefficient by a factor of 1.26. However, the increase of the apparent (observed) hydrodynamic radius of the same species in solution may differ from this value for structural/chemical reasons even assuming the absence of instrumental artifacts. From $D_{MC}$ of 0.2377 to $D_{2:1}$ of 0.2091, the change of D value for the **Eu-MC** system was found to be 1.14 vs a theoretical 1.26 value.

Among others, possible reasons for the divergence from theory are: presence of solvation molecules/solvation sphere, water exclusion at the contact interface of the two monomers, change in shape of the molecules (oblate molecules appear slower/bigger, prolate ones appear faster/smaller).

The factor of 0.12 difference between 1.26 (theoretical) and 1.14 (observed), translates into a difference in radius of ca. 0.7 Å between expectation and observation, which is less than a solvation peel around the MC dimer. Additionally, crystal structures of the 2:1 complex[8] (Scheme 1D) vs the monomer[9] (Scheme 1B) indicate that the shape of the monomer is much more oblate (disc shaped) whereas the 2:1 is more spherical, which could result in the monomer having more resistance to diffusion than the dimer and thus decrease the gap between monomer and dimer *D* parameters. A combination of solvent and shape effects could easily account for the departure of the results from theoretical expectations.

## Calculation of Hydrodynamic Radius by Stokes Einstein Equation

Given eq. 3 ($\frac{\theta_{an}}{\theta_{std}} = \frac{D_{an}}{D_{std}}$), once D of the analyte is known, $D_{an}$, the precise determination of the hydrodynamic radius $r_{an}$ for a substance in a given solvent comes down to the correct estimation or determination of the *c*, *T* and $\eta$ parameters in equation 1. As described by Zuccaccia and Macchioni,[10] use of an internal standard allows one to avoid determination of *T* or $\eta$, which are considered identical within a single experimental sample, and also allows one to bypass evaluation of *c*. However, the factor *c* is dependent on the sizes of the diffusing species, and should be estimated if the radii of the analyte and internal standard are not comparable. A suitable approximation of this factor has been described[11] by equation 8 that is based on the micro-friction theory of Wirtz and co-workers ($r_H = r_{an}$) in this treatment.[12]

$$c = \left( \frac{6}{1+0.695\left(\frac{r_{solv}}{r_{an}}\right)^{2.234}} \right) \qquad (8)$$

Combining this value for *c* with the Stokes Einstein equation (eq. 1) gives *D* of an analyte that is dependent both on hydrodynamic radius of the solvent $r_{solv}$ and on the analyte itself ($r_{an}$)

$$D = \frac{kT\left(1+0.695\left(\frac{r_{solv}}{r_{an}}\right)^{2.234}\right)}{6\pi\eta r_{an}} \qquad (9)$$

Combining equation 9 with equation 3, from PGSE data on a solution containing an analyte of unknown radius $r_{an}$ and an internal standard with radius $r_{std}$ in a solvent with radius $r_{solv}$, the following equation is obtained:

$$D'_{obs} = \frac{\theta_{an}}{\theta_{std}} = \frac{D_{an}}{D_{std}} = \left( \frac{1+0.695\left(\frac{r_{solv}}{r_{an}}\right)^{2.234}}{r_{an}} \right) * \left( \frac{r_{std}}{1+0.695\left(\frac{r_{solv}}{r_{std}}\right)^{2.234}} \right) \qquad (10)$$

The $\theta_{an}$ and $\theta_{std}$ exponential factors are determined from PGSE data. Using the Van der Waals radii of the internal standard (in our case DMSO, $r_{std}$ = 2.64 Å)[13] and of the solvent (in our case, the published hydrodynamic radius of methanol-$d_4$, $r_{solv}$ = 2.76 Å)[10] the value of $r_{an}$ (in our case $r_{MC}$) can be determined by iterative adjustment using Excel's Goal Seek solver, targeting to 0 the difference between the observed and calculated values, *i.e.*, the left and right sides of equation 10.

## Calculation of Error in Hydrodynamic Radius

Assuming that the uncertainties of $\theta_{MC}$ and $\theta_{std}$ exponential factors dominate over those of $r_{std}$ and $r_{solv}$, in terms of propagation of uncertainty if we have available a relationship in the form

$$r_{an} = f(\theta_{an}, \theta_{solv}) \qquad (11)$$

then an estimate of the standard deviation of $r_{an}$ can be calculated as

$$\sigma_{r_{an}} = \sqrt{\left(\frac{\partial f}{\partial \theta_{an}}\Big|_{\theta_{an}} \sigma_{\theta_{an}}\right)^2 + \left(\frac{\partial f}{\partial \theta_{std}}\Big|_{\theta_{std}} \sigma_{\theta_{std}}\right)^2} \qquad (12)$$

Unfortunately, equation 10 cannot be rearranged in the form of eq. 11, and therefore a different approach was used to derive such an equation. A Taylor expansion is used based on equation 10 to determine a polynomial function that approximates the value of $D'_{obs}$ for values of $r$ ($r_x$) close to $r_{an}$. Values a, b, and c are associated with a quadratic approximation at the point of interest $r_{an}$ with $r_x$ as the variable. Then these terms are used to rearrange the equation into the form of eq. 11 to calculate the projected error in radius based on the errors of the experimental $\theta_{an}$ and $\theta_{std}$ exponential factors.

We define the far right term in eq. 10 as $D'(r_x)$ function, which contains the radius of the analyte as the variable ($r_x$)

$$D'(r_x) = \left(\frac{1+0.695\left(\frac{r_{solv}}{r_x}\right)^{2.234}}{r_x}\right) \cdot \left(\frac{r_{std}}{1+0.695\left(\frac{r_{solv}}{r_{std}}\right)^{2.234}}\right) \qquad (13)$$

By virtue of eq. 10, also:

$$D'(r_{an}) = \frac{\theta_{an}}{\theta_{std}} = \frac{D_{an}}{D_{std}} \qquad (14)$$

the quadratic approximation of the function evaluated at the point $r_{an}$ is

$$D'(r_x) = D'(r_{an}) + [D'(r_{an})]'(r_x - r_{an}) + \frac{[D'(r_{an})]''}{2}(r_x - r_{an})^2 \qquad (15)$$

Where $D'(r_{an})$, $[D'(r_{an})]'$ and $[D'(r_{an})]''$ are the values of eq. 13, its first and second derivatives over $r_x$, calculated for $r_x = r_{an}$, respectively. By defining K as follows (a constant value throughout the Taylor expansion)

$$K = \frac{r_{std}}{1+0.695\left(\frac{r_{solv}}{r_{std}}\right)^{2.234}} \qquad (16)$$

the three parameters of the quadratic Taylor Expansion on equation 12 are calculated are as follows

$$D'(r_{an}) = K\left(\frac{1+0.695\left(\frac{r_{solv}}{r_{an}}\right)^{2.234}}{r_{an}}\right) = C \qquad (17)$$

$$[D'(r_{an})]' = K\left(\frac{-1617*0.695*{r_{solv}}^2\left(\frac{r_{solv}}{r_{an}}\right)^{\frac{117}{500}}}{500*{r_{an}}^4} - \frac{1}{{r_{an}}^2}\right) = B \qquad (18)$$

$$\frac{[D'(r_{an})]''}{2} = \frac{K}{2}\left(\frac{3423189*0.695*{r_{solv}}^2\left(\frac{r_{solv}}{r_{an}}\right)^{\frac{117}{500}}}{250000*{r_{an}}^5} + \frac{2}{{r_{an}}^3}\right) = A \qquad (19)$$

Rearranging eq.15, we obtain

$$a \cdot {r_x}^2 + b \cdot r_x + c = 0 \qquad (20)$$

Where coefficients *a*, *b* and *c* are defined through *A*, *B* and *C* (eq. 17-19) as follows

$$a = A \qquad (21)$$

$$b = B - 2Ar_{an} \qquad (22)$$

$$c = C - B \cdot r_{an} + A \cdot {r_{an}}^2 - D'(r_x) = c' - D'(r_x) \qquad (23)$$

It is worth noting that the function $D'(r_x)$ calculated for $r_x = r_{an}$ reduces to $D'(r_x) = C$, which is equivalent to equation 14, as expected.

Equation 20 is solved for $r_x$ according to $r_{x,\pm} = \frac{-b\pm\sqrt{b^2-4ac}}{2a}$

where, for $r_{solv} < r_{an}$, the solution with the minus sign is meaningful. Since values of $r_x$ very closely approximate values of $r_{an}$, it results $D'(r_x) \cong D'(r_{an}) = C$ and therefore:

$$r_{x,-} = \frac{-b-\sqrt{b^2-4ac}}{2a} = \frac{-b-\sqrt{b^2-4a\left(c'-\frac{\theta_{an}}{\theta_{std}}\right)}}{2a} \qquad (24)$$

which is in the desired form $r_{an} = f(\theta_{an}, \theta_{solv})$ (eq. 11). Following eq. 10 we can now calculate

$$\left.\frac{\partial f}{\partial \theta_{an}}\right|_{\theta_{an}} = -\frac{1}{\sqrt{4a\theta_{an}+\theta_{std}(b^2-4ac)}} = \frac{\sqrt{4a\theta_{an}-4ac\theta_{std}+b^2\theta_{std}}}{-\theta_{std}(b^2-4ac)-4a\theta_{an}} \quad (25)$$

$$\left.\frac{\partial f}{\partial \theta_{std}}\right|_{\theta_{std}} = \frac{(b^2-4ac)\sqrt{\frac{4a\theta_{an}-\theta_{std}(b^2-4ac)}{\theta_{std}}}}{4a(\theta_{std}(-b^2+4ac)-4a\theta_{an})} + \frac{\sqrt{\frac{4a\theta_{an}-\theta_{std}(b^2-4ac)}{\theta_{std}}}}{4a\theta_{std}} \quad (26)$$

The standard deviation of radius $r_{an}$ is eventually determined through eq. 12, by considering the values obtained in eq. 25 and 26, and the standard deviations of the decay parameters $\theta_{an}$ and $\theta_{std}$.

**Complexation for All Lanthanides Tested**

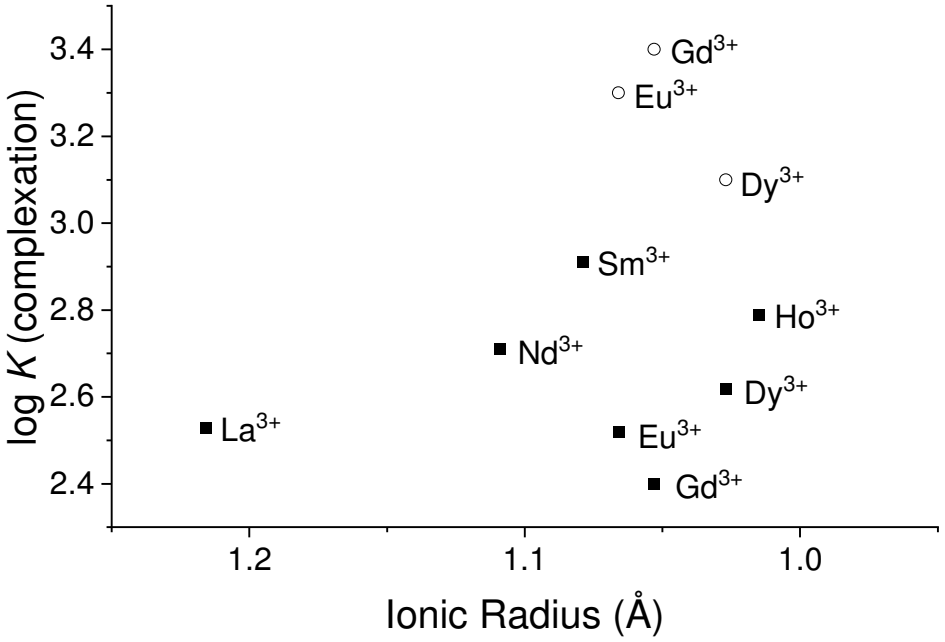


**Figure S13.** Summary of Log *K* according to lanthanide species ionic radius, including all seven **Ln-MC** species examined, where the radius for $La^{3+}$ is for a 9-coordinate species and the remaining lanthanides are 8-coordinate.[14] Black squares: $K_1$ values to describe the equilibrium **MC** + Muc ⇄ (**MC**)Muc; Open circles: $K_2$ values to describe the equilibrium **MC** + (**MC**)Muc ⇄ (**MC**)$_2$Muc

[1] A. Pavlishchuk, D. Naumova, M. Zeller, S. Calderon Cazorla, A. W. Addison, *Acta Crystallographica Section E* **2019**, *75*, 1215-1223.

[2] C. M. Zaleski, C.-S. Lim, A. D. Cutland-Van Noord, J. W. Kampf, V. L. Pecoraro, *Inorg. Chem.* **2011**, *50*, 7707-7717.

[3] C. Sgarlata, A. Giuffrida, E. R. Trivedi, V. L. Pecoraro, G. Arena, *Inorg. Chem.* **2017**, *56*, 4771-4774.

[4] T. Stait-Gardner, P. G. Anil Kumar, W. S. Price, *Chem. Phys. Lett.* **2008**, *462*, 331-336.

[5] a) A. Pacco, T. N. Parac-Vogt, E. van Besien, K. Pierloot, C. Görller-Walrand, K. Binnemans, *Eur. J. Inorg. Chem.* **2005**, *2005*, 3303-3310; b) T. N. Parac-Vogt, A. Pacco, C. Görller-Walrand, K. Binnemans, *J. Inorg. Biochem.* **2005**, *99*, 497-504.

[6] A. K. Covington, M. Paabo, R. A. Robinson, R. G. Bates, *Anal. Chem.* **1968**, *40*, 700-706.

[7] Hyperquad Simulation and Speciation Protonic Software. Available online: http://www.hyperquad.co.uk/hyss.htm, 2009.

[8] C. S. Lim, A. C. V. Noord, J. W. Kampf, V. L. Pecoraro, *Eur. J. Inorg. Chem.* **2007**, *2007*, 1347-1350.

[9] A. D. Cutland, J. A. Halfen, J. W. Kampf, V. L. Pecoraro, *JACS* **2001**, *123*, 6211-6212.

[10] D. Zuccaccia, A. Macchioni, *Organometallics* **2005**, *24*, 3476-3486.

[11] a) H. C. Chen, S. H. Chen, *The Journal of Physical Chemistry* **1984**, *88*, 5118-5121; b) P. J. Espinosa, J. Garcia de la Torre, *J. Phys. Chem.* **1987**, *91*, 3612-3616.

[12] a) A. Spernol, K. Wirtz, *Zeitschrift für Naturforschung A* **1953**, *8*, 522-532; b) A. Gierer, K. Wirtz, *Zeitschrift für Naturforschung A* **1953**, *8*, 532-538.

[13] K. Rah, S. Kwak, B. C. Eu, M. Lafleur, *J. Phys. Chem. A* **2002**, *106*, 11841-11845.

[14] R. D. Shannon, *Acta Crystallogr. Sect. A* **1976**, *32*, 751-767.